RSC Advances

PAPER

View Article Online
View Journal | View Issue

Cite this: *RSC Adv.*, 2026, **16**, 9143

An investigation of electrocatalytic activity of the FeCe nanoparticle encapsulated carbon nanotube towards oxygen reduction reaction

Dikeshwar Halba, [a] Lokesh Yadav [a] and Srimanta Pakhira *[ab]

The sluggish O_2 reduction reaction (ORR) that occurs in fuel cells requires an efficient electrocatalyst to increase the efficiency of the fuel cells. It is necessary to replace the widely acknowledged Pt-based electrocatalyst with a low-cost, non-precious metal-based electrocatalyst to efficiently catalyze the ORR. Herein, we propose a material comprising Fe–Ce nanoparticles encapsulated within a carbon nanotube, *e.g.*, FeCe@CNT, as a promising electrocatalyst for the ORR. The structural and electronic properties, *i.e.*, electronic band structure and total density of states (DOS), of the FeCe@CNT material were studied by employing a first-principles-based DFT-D3 method. Our current study found that the FeCe@CNT material has conducting properties due to its zero electronic band gap (E_g). The electronic bands cross the Fermi energy level (E_F) with a large electron density of states around the Fermi level in total DOS, confirming the conducting nature of the subject material. This study explored all the reaction steps involved in the ORR mechanism on the surface of the FeCe@CNT system. The O_2 adsorption on the surface of the FeCe@CNT system occurred with an adsorption energy (ΔE) of −1.67 eV. This study found that the ORR mechanism on the surface of the FeCe@CNT material proceeds through the four-electron ($4e^-$) transfer mechanism. The associative pathway of the ORR, along with various reaction intermediates, was explored using the adsorption energy. Our energy calculation demonstrates that the active sites on the FeCe@CNT material are thermodynamically favorable for catalyzing the ORR. Our study found that the FeCe@CNT material is a potential candidate that can be used in the fuel cell as a cathodic electrode material. The valuable insights from the strong FeCe nanoparticle interaction with the CNT will help advance the interfacial design of novel electrocatalysts towards the ORR.

Received 22nd January 2026
Accepted 27th January 2026

DOI: 10.1039/d6ra00601a

rsc.li/rsc-advances

Introduction

Fossil fuels are a major energy source that fulfills the global energy demands, leading to increased greenhouse gas (*e.g.*, CO_2 and CO) emissions.[1–4] Fuel cells and metal-air batteries (MABs) are considered to be the most promising renewable energy-converting devices due to their high efficiency, high power density, low operating temperature, and low carbon emissions.[5–8] In fuel cells, the ORR is a crucial process that takes place at the cathode. The sluggish ORR kinetics influence the overall efficiency of the fuel cell, which can either occur through four-electron ($4e^-$) or two-electron ($2e^-$) transfer mechanism pathways.[9–11] The hydrogen oxidation ($H \rightarrow H^+ + e^-$) at the anode is an easy process involving a single electron transfer process, in contrast to the cathode where a cascade of reactions takes place. Fuel cells require an efficient electrocatalyst to catalyze the sluggish ORR to improve its performance. To date, precious Pt-based materials are considered to be the best electrocatalysts for the ORR due to their high catalytic activity and low overpotential.[12–14] The high cost, low stability, and intolerance to the fuel crossover are the major parameters that hinder the widespread commercialization of Pt-based electrocatalysts on large-scale applications. Hence, it is important to explore new low-cost, stable, and efficient electrocatalysts based on non-precious materials for catalyzing the ORR to attain the full potential of fuel cells in large-scale applications.[15–18]

In recent decades, various electrocatalysts for ORR have been explored by researchers, including carbon-based materials such as carbon nanotubes (CNTs) and nitrogen-doped carbon nanotubes (NCNTs) due to their unique property. The CNTs have shown excellent catalytic activity for ORR in fuel cells. Chen *et al.* found that NCNTs exhibited high ORR activity comparable to that of platinum-based catalysts.[19] The encapsulation of a nanocluster within CNTs has received significant attention from researchers.[20–23] Recently, Niu *et al.* found that the CoNi@NCNT/NF material showed excellent electrocatalytic

[a]*Theoretical Condensed Matter Physics and Advanced Computational Materials Science Laboratory, Department of Physics, Indian Institute of Technology Indore (IIT Indore), Simrol, Khandwa Road, Indore, Madhya Pradesh, 453552, India. E-mail: spakhira@iiti.ac.in; spakhirafsu@gmail.com*

[b]*Theoretical Condensed Matter Physics and Advanced Computational Materials Science Laboratory, Centre for Advanced Electronics (CAE), Indian Institute of Technology Indore, Simrol, Khandwa Road, Indore, Madhya Pradesh, 453552, India*

activity for ORR and HER.[24] It was experimentally found that the Ni_3Fe nanoalloy encapsulated within CNT/NCNT demonstrated excellent electrocatalytic activity for HER.[25] The synergic effect between the encapsulated metal nanoparticle and CNT/NCNT makes these materials a good cathodic material for ORR by improving the electronic properties. The interaction between the CNT and nanoparticle reduces the activation energy barrier and increases the stability during the chemical reaction.[26] It was observed that high ORR activity and stability are achieved because of the transition metal centers (*e.g.*, Cu, Fe, and Co) in the metal nanoparticle encapsulated in CNT.[27] Yang *et al.* found that iron/iron carbide (Fe/Fe_3C) encapsulated in CNTs showed good bifunctional electrocatalytic activity for ORR and OER.[28] Recently, Zhao *et al.* synthesized Fe_3N nanoparticle-encapsulated NCNT on the surface of a flexible carbon cloth, *e.g.*, Fe_3N@NCNT/CC, and they found that it showed satisfactory ORR performance.[29] Recently, Singh and Pakhira theoretically studied the Co nanoparticle-encapsulated single-walled carbon nanotube (Co@SWCNT) and found that it has excellent catalytic activity for ORR.[30] Similarly, in our recent previous work, we found that the CoPt@CNT material showed excellent catalytic activity for the ORR mechanism.[31] This experimental and theoretical research inspired us to explore and study new non-noble metal-based electrocatalysts for ORR, namely the FeCe@CNT material. Materials incorporating precious metals such as platinum (Pt) or platinum group metals (PGMs) with their alloys have demonstrated exceptional electrocatalytic properties in electrochemical systems, particularly in fuel cells. However, the scarcity, high cost, and low selectivity of PGM catalysts seriously impede their large-scale application. Therefore, developing non-PGM catalysts with high ORR activity and durability is of great interest. To address these issues, we have computationally designed a Pt-free FeCe@CNT material, and investigated its electronic properties and electrocatalytic activities towards ORR.

In the present study, we have investigated the subject material FeCe@CNT as a potential candidate for catalyzing the O_2 reduction reaction. At the beginning, we studied the equilibrium structure and electronic properties of a pristine carbon nanotube (CNT). We found that the pristine CNT is metallic in nature, as there is a large electron density around the Fermi level (E_F). Then, we computationally encapsulated Fe–Ce nanoparticles within the equilibrium structure of the pristine CNT to make our studied material FeCe@CNT. The motivation for incorporating cerium (Ce) with iron (Fe) in our current work is due to Ce's unique electronic and redox properties. Some studies reported that the cerium-based catalysts have high ORR/OER performance due to the redox activity and oxygen vacancy formation.[32,33] The synergistic effect is achieved when the Ce atom is incorporated with the Fe in the carbon nanotubes (CNTs), where the Ce generally enhances the electronic environment of the Fe atoms towards the subject reaction, *i.e.*, ORR. The combination of Fe and Ce nanoparticles increases the electronic structure of the outer carbon wall in the FeCe@CNT material for efficient O_2 adsorption. Various studies have emphasized the significance of the synergistic interaction between encapsulated nanoparticles and CNTs, providing a valuable concept for developing well-stabilized electrocatalysts.[34] Experimentally, it was found that the Ce doping in N-doped carbon frameworks demonstrates excellent ORR activity and durability.[35] Bi *et al.* found that the synergistic effect of Co and Pt with the carbon support enhances the electrocatalytic activity of $CoPt_3$@NC for HER and OER.[36] Recently, Singh and Pakhira theoretically explored the ORR mechanism on the surface of the Co@SWCNT material.[30] Theoretically and experimentally, Niu *et al.* designed and studied the catalytic activity of CNTs and NCNTs encapsulating the CoNi nanocluster, which enhances the ORR activity of the CoNi@NCNT material.[24] These theoretical and experimental works have motivated us to explore the FeCe@CNT material for ORR. We hope that future experimental work will focus on synthesizing well-defined FeCe@CNT and other CNT-based materials for fuel cell applications towards ORR.

We thoroughly analyzed the equilibrium geometry and studied the electronic properties, *i.e.*, electronic band structure, electronic band gap (E_g) and total electronic density of states (TDOS), of the FeCe@CNT material. In the TDOS, a large electron density of states around the Fermi energy level (E_F) confirms the conducting nature of the FeCe@CNT material, which is essential for an electrocatalyst towards ORR. We found that the FeCe@CNT's catalytic activity emerges due to the synergic effect between the carbon nanotube and Fe–Ce nanoparticle. After confirming the conducting nature of the FeCe@CNT material, we started to explore both the associative and dissociative ORR mechanisms to investigate its electrocatalytic activity. We studied each reaction intermediate of the ORR mechanism by calculating their adsorption energy (E_{ads}). In this study, we have not discussed the dissociative mechanism because the energy required during the O_2 dissociation step ($O_2^* \rightarrow 2O^*$) was highly positive, which is unfavorable for the initiation of the ORR. The positive value of the adsorption energy in the case of the O_2 dissociation step signifies that an input of external energy is needed for this step to occur, which is thermodynamically and energetically unfavorable for the ORR. Hence, this study focused on the associative mechanism and calculation of the relative adsorption energy of all the reaction intermediates involved in the ORR mechanism. Our adsorption energy (ΔE) calculations show that the formation of the reaction intermediates at successive steps is spontaneous and energetically feasible during the ORR. Our study demonstrated that the subject material FeCe@CNT is an excellent ORR electrocatalyst. So, our studied FeCe@CNT material can be a potential electrode material in fuel cells for efficiently reducing oxygen molecule to water.

Mechanism of the O_2 reduction reaction

In electrochemical energy conversion devices like fuel cells, proper knowledge of the ORR mechanism is vital for exploring an efficient electrocatalyst. The ORR mechanism proceeds either through a direct $4e^-$ transfer mechanism or an indirect $2e^-$ transfer mechanism. The ORR $4e^-$ transfer mechanism includes the reduction of an oxygen (O_2) molecule with four electrons (e^-) and four protons (H^+) to produce two water (H_2O)

molecules. In contrast, the $2e^-$ transfer mechanism involves the reduction of the O_2 molecule with two electrons and two protons, where we get hydrogen peroxide (H_2O_2) as a product.[37,38] The formation of the H_2O_2 product *via* the $2e^-$ path makes the fuel cell less efficient because it affects the overall kinetics of the reaction. The $4e^-$ path of ORR in the acidic medium includes a dissociative path where O_2 dissociates or an associative path where hydrogenation of O_2 takes place. The ORR mechanism *via* associative path is given below,

$$O_2 + * \rightarrow O_2*$$

$$O_2* + H^+ + e^- \rightarrow OOH*$$

$$OOH* + H^+ + e^- \rightarrow O* + H_2O$$

$$O* + H^+ + e^- \rightarrow OH*$$

$$OH* + H^+ + e^- \rightarrow * + H_2O \quad (1)$$

In the above equation, * represents the favorable active site where the adsorption of an O_2 molecule occurs. Here, the protons (H^+) and electrons (e^-) were added with the oxygen molecule to produce water in the successive step of ORR.

Computational details

The equilibrium crystal structure, electronic properties, band structure, and TDOS were computed using the first principle-based hybrid periodic density functional theory (DFT).[39–41] All DFT calculations were performed using the CRYSTAL 17 suite code.[42–44] The B3LYP-D3 method was employed in the current study to obtain the equilibrium structures and to explore the reaction mechanisms.[40,41] Grimme's weak 3rd order dispersion corrections (–D3) are used to account for long-range van der Waals interactions.[45,46] Here, Gaussian-type basis sets were used in the *ab initio*-based CRYSTAL17 suite code to describe the atomic orbitals. Furthermore, spin polarized calculations were performed to find the equilibrium structure and analyze the electronic properties of the studied material. The basis sets used for Fe and C atoms were of triple-ζ valence with polarization quality Fe_pob_TZVP_2012 and C_pob_TZVP_2012. The effective core potential Ce_ECP_Meyer_2009 was used for the Ce atom. The choice of functional and the use of an effective core potential (ECP) for the Ce atom were carefully selected to provide a balance between accuracy and computational efficiency. Kullgren *et al.* showed that the small-core Ce ECPs give accurate CeO_2 structures and energies, matching all-electron results within ~0.1 eV in their study.[47] Zhang *et al.* evaluated small-core Ce ECPs for defect formation energies in CeO_2.[48] The chosen functional captures the essential electronic and redox properties of Ce, while the ECP effectively models core electrons, incorporating relativistic corrections for the Ce's 4f states, which enable a feasible treatment of this heavy element. While some minor relativistic and correlation effects may not be fully captured, this method is well-validated. This provides a reliable framework for investigating the Ce's role in the FeCe@CNT material. In our present calculation, the Monkhorst–Pack method was employed to integrate the Brillouin zone.[49] A $4 \times 4 \times 8$ Monkhorst–Pack *k*-point grid was used for the structural optimization of the subject material. The "ATOMSPIN" and "SPINLOCK" keywords are used to define the electron occupancy for either spin up or spin down in the *ab initio* CRYSTAL 17 program.[50,51] A visualization software VESTA was used to visualize the equilibrium structure of various reaction intermediates.[52] The atomic orbitals of Fe, C, and Ce atoms were used to compute the TDOS of the FeCe@CNT material during the present calculation.

Theoretical calculation and equation

In the present study, we studied the electrocatalytic activity of the FeCe@CNT material by exploring the ORR mechanism on its surface. Each reaction intermediate step was thoroughly studied by calculating the adsorption energy of every adsorbate, which is given by the following eqn (2),

$$E_{ads} = E_{adsorbate/FeCe@CNT} - E_{FeCe@CNT} - E_{adsorbate} \quad (2)$$

Here, in the above eqn (2), $E_{adsorbate/FeCe@CNT}$ represents the total energy of the FeCe@CNT system with the adsorbate, and $E_{FeCe@CNT}$ and $E_{adsorbate}$ are the energies of the FeCe@CNT system and adsorbate entity, respectively. A chemical reaction is said to be exothermic if the adsorption energy is negative because no external energy input is required for the reaction step to occur. A negative adsorption energy is energetically favorable during the subject reaction because energy is released, which can be used to drive the other reaction steps.

In the present study, the thermodynamic analysis of the ORR pathway on the FeCe@CNT material is entirely based on the adsorption energy (ΔE), rather than fully corrected Gibbs free energies (ΔG). The reported overpotential in this work is estimated using ΔE as an approximation to ΔG within the computational hydrogen electrode (CHE) framework. Zero-point energy and entropic corrections were not included in the present calculations. This method is common when the goal is to compare the relative activity of similar catalysts because these missing corrections tend to influence all reaction steps by similar amounts. Therefore, even though the absolute values may not be exact, the trends and identification of the key reaction step remain reliable. A more detailed analysis would involve incorporating zero-point energy and entropic contributions to accurately plot the full free-energy diagrams of the ORR pathway, which provides a valuable direction for further research and a deeper understanding.[37,53,54] It demands a rigorous computing resource and computing times, and such detailed analysis has been left for future work.

Results and discussions

A 3D periodic unit cell was employed to model the FeCe@CNT structure. The FeCe@CNT model consists of a Fe_3Ce nanocluster (Fe : Ce = 3 : 1) encapsulated within a (6, 6) armchair single-walled carbon nanotube (tube diameter ≈ 9.35 Å, $a = b =$

21.65 Å, $c = 2.49$ Å). The initial geometry positions a central Ce atom at the CNT axis (0, 0, 0) surrounded by three symmetry-equivalent Fe atoms in a tetrahedral-like configuration (maximum Fe–Fe distance ≈ 5.24 Å) at $z = -0.5$, ensuring complete encapsulation with a lateral separation that is greater than 15 Å between the periodic images. The electronic properties of the equilibrium FeCe@CNT material were studied employing the B3LYP-D3 (*i.e.*, DFT-D3) method. We have considered a unit cell of the van der Waals (vdW) crystal to present both the CNT and FeCe@CNT materials in the present investigation, so that the computations and analysis can be easily performed by imposing the symmetry in the CRYSTAL17 suite code.[54–57] The equilibrium structure of the FeCe@CNT material is depicted in Fig. 1a, and it has a hexagonal $P\bar{6}$ space group symmetry. The equilibrium lattice parameter of the vdW crystal structure of the subject material, *i.e.*, the lattice constants and bond angles of the FeCe@CNT material, were found to be $a = b = 21.65$ Å, $c = 2.49$ Å, and $\alpha = \beta = 90°$, $\gamma = 120°$ respectively. The electronic band structure calculations and total density of states (TDOS) of the FeCe@CNT material are depicted in Fig. 1b, which was computed by employing a highly symmetric Γ–K–M–L–A–H–L–Γ *k*-vector direction. Our study has found that the FeCe@CNT material is metallic in nature as some electronic energy bands overlap with each other and cross the Fermi energy level (E_F), as shown in Fig. 1b. The metallic nature of the FeCe@CNT material is clear from its TDOS calculations shown in Fig. 1b due to the presence of a significant electron density of states at the Fermi energy level (E_F). The synergic effect between the Fe–Ce nanoparticle and carbon nanotube (CNT) makes the FeCe@CNT material an excellent catalytic material because mass electron and charge transfer becomes easy during the chemical reaction. The electron density from the d-subshell of Fe and Ce atoms contribute to the TDOS of the FeCe@CNT material, which makes it a conducting material, as shown in Fig. 1c. Furthermore, after confirming the conducting nature of FeCe@CNT, the ORR mechanism on the surface of the FeCe@CNT material has been explored based on the computational hydrogen electrode (CHE) model.

Previous studies have experimentally synthesized Co@SWCNT and investigated its catalytic applications, including the hydrogen evolution reaction (HER) and lithium–sulfur batteries, using both experimental and theoretical approaches.[58,59] Similarly, cobalt-encapsulated nitrogen-doped carbon nanotubes have been experimentally synthesized, and their applications towards the ORR and OER have been reported.[60–62] Experimentally, Fe/N-doped carbon nanotubes (Fe/N-CNTs) were synthesized using the one-pot grinding-calcination of iron salts with CNTs and nitrogen precursors. Fe/N-CNTs demonstrated an excellent ORR performance in microbial fuel cells and alkaline media.[63] Wang *et al.* experimentally synthesized Ce-doped Fe–N–C/Fe_3C nanosheets by ZIF-assisted molten salt pyrolysis method, and they found that it exhibited enhanced bifunctional ORR/OER performance due to synergistic Fe-Nx and Ce–N active sites.[64] Our current study is purely based on theoretical work, whereas precise FeCe@CNT remains unexplored experimentally. The encapsulation of FeCo alloy nanoparticles inside CNTs is achieved by the CVD method and explored for catalysis.[65] These experimental studies (bimetallic encapsulation *via* CVD/pyrolysis method) indicate that the FeCe@CNT material is synthetically plausible, although there are no direct reports. However, controlling bimetal dispersion to prevent aggregation, achieving uniform encapsulation for stability under ORR conditions, and scaling beyond laboratory synthesis are the main challenges during the synthesis process. Future experimental synthesis and ORR performance validation of FeCe@CNT are anticipated, guided by established bimetallic CNT encapsulation precedents. This study provides detailed mechanistic insights into the ORR mechanism *via* the DFT-D3 method. Our work is inherently theoretical and lacks direct experimental comparison, and it suggests an experimental

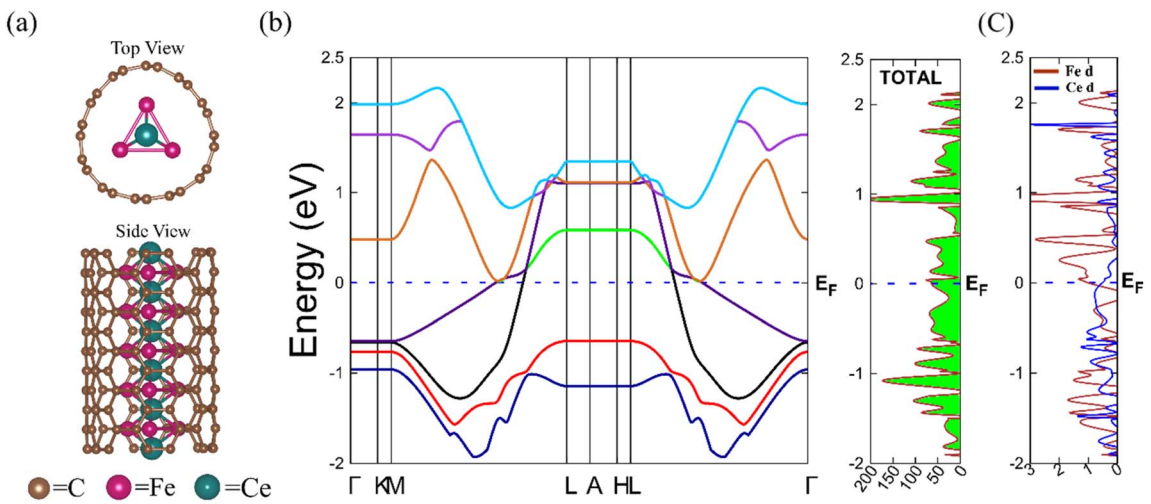

Fig. 1 (a) Top and side views of the equilibrium structure of the FeCe@CNT, (b) electronic band structure and the total DOS of the FeCe@CNT material, and (C) PDOS depicting the contribution from the d subshell electron density of Fe and Ce atoms.

approach for synthesizing the system and studying the ORR activity.

In this work, Mulliken charge analysis of the FeCe@CNT system was performed to understand the nature and extent of charge transfer within the material. From the Mulliken charge analysis, we found that the main charge transfer occurs from the Ce to the Fe atoms, with each Fe gaining electronic charges of about 0.3–0.4 |e| and Ce losing charges of roughly one electron in total. Also, a part of this charge is further delocalized from the Fe atoms to the adjacent carbon atoms in the FeCe@CNT material. This charge redistribution shows that the encapsulated Fe–Ce cluster acts as an electronic promoter that increases the nearby CNT carbon surface with electrons. Hence, the carbon sites on the CNT surface act as the primary active centers for O_2 adsorption during the ORR. The overall ORR on the FeCe@CNT surface is efficiently promoted by the charge transfer between the encapsulated Fe–Ce cluster and the surrounding carbon network. While Bader charge and COHP analysis offer valuable complementary perspectives, Mulliken population analysis adequately supports our qualitative discussion of the electronic structure, as commonly applied in similar DFT studies on ORR. In the CRYSTAL17/23 suite code, Bader charge analysis option is not supported. Hence, we have carried out Mulliken charge analysis of the subject material.

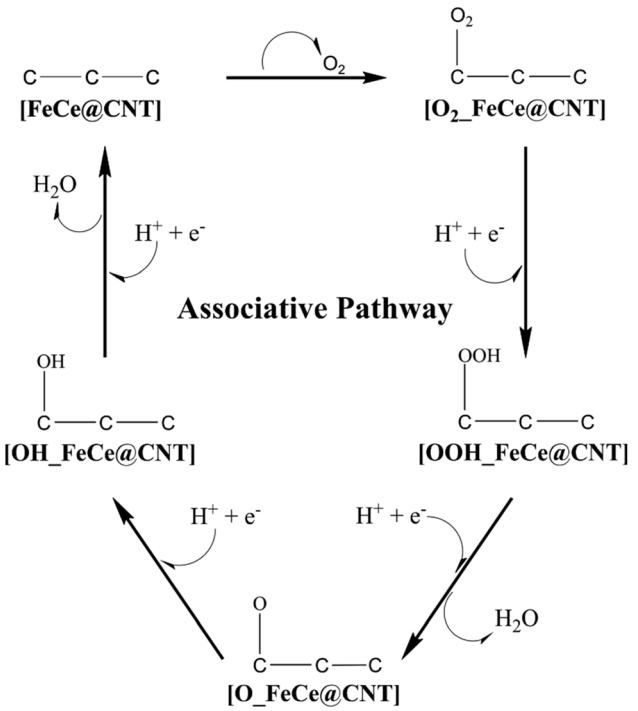

Fig. 2 Schematic of the associative four-electron transfer pathway on the FeCe@CNT surface.

ORR mechanism

The O_2 adsorption on the surface of the catalytic material at the active site is the initial step of the ORR mechanism. After the adsorption of the O_2 molecule, a successive reaction occurs on the surface of the catalyst, which involves the addition of protons (H^+) and electrons (e^-) with the O_2 molecule to form the water (H_2O) molecule in the ORR. In the whole ORR, a total of four electrons ($4e^-$) and four protons ($4H^+$) are simultaneously utilized to reduce an O_2 molecule to $2H_2O$ molecules. The ORR mechanism was investigated on the surface of the FeCe@CNT material based on the computational hydrogen electrode (CHE) model. Fig. 2 depicts the schematic representation of the $4e^-$ transfer mechanism of associative ORR on the FeCe@CNT surface.

Step 1. O_2 adsorption. The very first step of the ORR mechanism is the O_2 molecule adsorption on the surface of the FeCe@CNT material, as shown in Fig. 2. The O_2 molecule gets attached to the carbon (C) atom on the surface of the FeCe@CNT material, which leads to the generation of the O_2-_FeCe@CNT reaction intermediate. We analyzed the equilibrium structure of the O_2_FeCe@CNT reaction intermediate and studied its electronic properties by using the DFT-D3 method. We found that the equilibrium structure of the O_2_FeCe@CNT reaction intermediate has hexagonal $P\bar{6}$ space group symmetry, as depicted in Fig. 3a. The equilibrium lattice parameters of the O_2_FeCe@CNT reaction intermediate were $a = b = 21.59$ Å, $c = 2.51$ Å, and $\alpha = \beta = 90°$, $\gamma = 120°$, respectively, obtained by the DFT-D3 method. The equilibrium C–C and C–O bond distances were 1.44 Å and 2.87 Å, respectively, computed at the same level of theory. The electronic band structure and TDOS of the O_2-_FeCe@CNT reaction intermediate were calculated by using a highly symmetric Γ–K–M–L–A–H–L–Γ path, and it is depicted in Fig. 3b. In the TDOS, a small electron density exists near the Fermi energy level (E_F). Also, a few bands cross and overlap above the Fermi level, which shows the excellent conductivity of the O_2_FeCe@CNT reaction intermediate for electron and charge transfer during the ORR. Our DFT study reveals that the electronic band gap of the O_2_FeCe@CNT intermediate is zero, resulting in it being purely conducting in nature. The O_2 adsorption on the surface of the FeCe@CNT material occurred with a cost of energy −1.67 eV. The negative value of adsorption energy in the O_2 adsorption step signifies that the formation of O_2_FeCe@CNT from the FeCe@CNT intermediate is spontaneous. No external input of energy is needed for the occurrence of this step, and it is energetically feasible.

Liu *et al.* found that the nickel-iron nanoparticle encapsulated in carbon nanotubes (NiFe@CNTs) demonstrated excellent ORR activity.[66] Recently, we have proposed CoPt@CNT as an excellent electrocatalytic material for ORR using the DFT method. The excellent catalytic activity of CoPt@CNT is due to the synergetic effects between the CoPt nanoparticle and carbon nanotube (CNT).[31] Similarly, in the FeCe@CNT material, the synergetic effect promotes better electron transfer and high stability during the ORR, and the costly element Pt has been removed. In some studies, remarkable ORR performance has been shown by encapsulating the first-row transition metal nanoparticles (*e.g.*, Fe, Co, Ni) in nitrogen-doped CNTs (NCNTs).[67] The electrons are transferred from the encapsulated metal core to the N-doped carbon wall, which tunes the local electronic structure of the carbon surface that facilitates easy ORR activity. In FeCe@CNT, the intimate contact between the

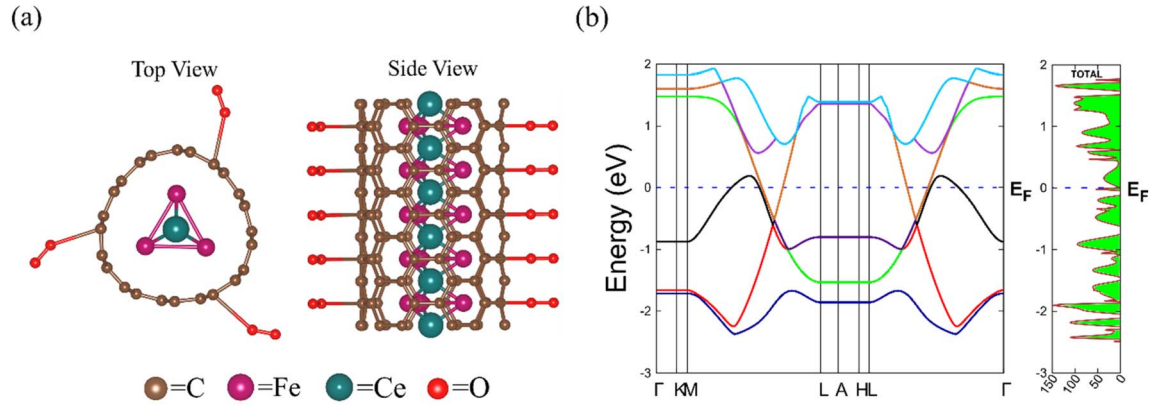

Fig. 3 (a) Top and side views of the equilibrium structure of O_2_FeCe@CNT, and (b) the electronic band structure and the total DOS of the O_2_FeCe@CNT reaction intermediate.

FeCe nanoparticle and the CNT surface induces electronic interactions that optimize the adsorption energy for ORR intermediates. A theoretical study conducted by Deng *et al.* on the Fe-encapsulated single-walled carbon nanotube (Fe@SWCNT) proposed that the O_2 adsorption energy on the pristine Fe@SWCNT was +0.03 eV.[68] Ulbricht *et al.* experimentally found that the adsorption energy of the O_2 molecule on SWCNT was +0.80 eV.[69] Recently, Singh and Pakhira proposed that the O_2 adsorption energy on the Co@SWCNT material was +0.15 eV.[30] In our recent study, we found that the O_2 adsorption on CoPt@CNT takes place with an adsorption energy of −0.79 eV.[31] In this study, the O_2 adsorption energy on the FeCe@CNT material was −1.67 eV, which is negative. The lower value of O_2 adsorption energy for FeCe@CNT (−1.67 eV) signifies the easy and stable adsorption of O_2 on the CNT surface. The O_2 adsorption on the FeCe@CNT surface is exothermic and energetically favorable during the initial stage of the ORR mechanism. These results confirm that our subject material FeCe@CNT is a novel material that can be used in the fuel cell for efficiently catalyzing the ORR.

Chen *et al.* employed a (6, 6)-CNT model with Fe–N_4 active sites in supercells of 24–48C atoms. A single ORR intermediate (*O/*OH) per cell resulted in ∼6–9 Å periodic spacing between sites. They found that the calculated adsorption energies matched graphene benchmarks despite the CNT curvature, without applying lateral interaction corrections.[70] Kuzmin *et al.* modeled M-N_4-doped (6, 6)-SWCNT (M = Cu, Ag, Zn) in ∼24C atom cells, with the ORR intermediate (*OOH/*OH) adsorbed on adjacent C/N sites at <6 Å.[71] Their study revealed that full ORR free-energy profiles were obtained without larger supercells, suggesting minimal lateral interactions at these low spacings. These studies confirm ORR intermediates adsorb at close distances (6–9 Å periodic, <6 Å local) without significant interference, as evidenced by validated adsorption energies and full mechanistic profiles. The FeCe@(6, 6)-CNT (9.35 Å diameter) follows this established methodology for studying the ORR mechanism. Our (6, 6)-CNT model encapsulating Fe–Ce nanocluster, with a diameter of 9.35 Å, aligns with the work from Niu *et al.*, who showed that smaller CNT diameters produce tighter circumferential spacing of active sites (∼7–9 Å) due to enhanced curvature.[24] Thus, the chosen unit cell size and active site density ensure reliable DFT-D predictions of ORR thermodynamics and kinetics of the subject FeCe@CNT material, consistent with literature precedents and curvature effects. Our model is a well-established model that we have used in our previous studies. Other groups have also published their works with the experimental validation.

Step 2. formation of the OOH intermediate. The next step of ORR follows the protonation of the O_2 molecule attached to a carbon atom on the surface of the FeCe@CNT material. Fig. 4a shows the optimized structure of the OOH_FeCe@CNT reaction intermediate. The OOH_FeCe@CNT reaction intermediate forms when an electron (e^-) and proton (H^+) react with the attached O_2 molecule on the surface of the O_2_FeCe@CNT intermediate. This reaction step occurred with an adsorption energy of −0.10 eV. Here, the negative adsorption energy signifies that this reaction step is energetically feasible. The equilibrium structure of the OOH_FeCe@CNT intermediate exhibits $P\bar{6}$ space group symmetry. It was determined that the lattice parameter of the equilibrium OOH_FeCe@CNT intermediate measures $a = b = 21.85$ Å, $c = 2.50$ Å, and $\alpha = \beta = 90°$, $\gamma = 120°$, respectively, computed by the same DFT-D3 method. The equilibrium C–C and C–O bond lengths were found to be 1.61 Å and 1.46 Å obtained by the same level of theory. Additionally, the equilibrium O–H bond length was calculated to be 0.97 Å. Our present study on the electronic properties of the OOH_FeCe@CNT reaction intermediate reveals that it has a zero band gap. The electronic band structure and TDOS of the OOH_FeCe@CNT intermediate are represented in Fig. 4b. A highly symmetric Γ–K–M–L–A–H–L–Γ path was utilized to plot the electronic band structures of the OOH_FeCe@CNT reaction intermediate. In the band structure calculations, we can see some bands overlapping with each other and a small electron density is present near the Fermi energy level (E_F) in the TDOS, which signifies the conducting nature of the OOH_FeCe@CNT reaction intermediate, as depicted in Fig. 4b. The equilibrium lattice parameter, lattice constant and space group symmetry of

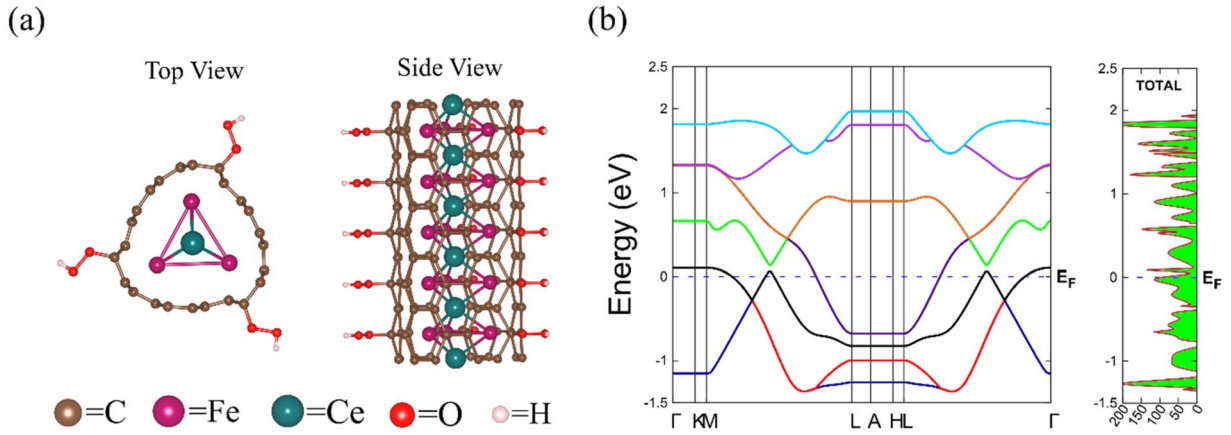

Fig. 4 (a) Equilibrium structure (top and side views) of OOH_FeCe@CNT, and (b) the electronic band structure and the total DOS of the OOH_FeCe@CNT reaction intermediate of the ORR mechanism obtained by the DFT-D3 method.

all the reaction intermediates of the ORR mechanism are listed in Table 1.

Step 3. removal of the first H_2O molecule. In the next step, one more electron and proton simultaneously react with the OOH_FeCe@CNT reaction intermediate to generate the first water molecule, and a new reaction intermediate O_FeCe@CNT is formed. Here, the hydroxyl group (OH^-) attached to the FeCe@CNT surface combine with a proton and electron to form a water molecule. The reaction intermediate O_FeCe@CNT formed from the OOH_FeCe@CNT intermediate with an adsorption energy of about −2.59 eV. The negative adsorption energy value in this step signifies that it is thermodynamically and energetically favorable for ORR. No additional energy is required during this step to occur as it is an exothermic reaction. The O_FeCe@CNT reaction intermediate has only one activated oxygen atom attached to the surface of the FeCe@CNT material, as depicted in Fig. 5a. This study has found that the equilibrium structure of the O_FeCe@CNT reaction intermediate has a hexagonal $P\bar{6}$ symmetry. The equilibrium lattice parameters of the O_FeCe@CNT material were found to be $a = b = 22.84$ Å, $c = 2.48$ Å, and $\alpha = \beta = 90°$, $\gamma = 120°$, respectively, computed by the DFT-D level of theory. The equilibrium C–C and C–O bond distances were 1.48 Å and 1.35 Å, respectively. The electronic band structure and TDOS of the O_FeCe@CNT reaction intermediate are displayed in Fig. 5b, which were computed using the high symmetric Γ–K–M–L–A–H–L–Γ direction. A small electron density near the Fermi energy level (E_F) in the TDOS confirms the semiconducting nature of the O_FeCe@CNT intermediate, which favors the reaction process for the easy transfer of electron and charge.

Step 4. formation of the OH reaction intermediate. The next step of the associative mechanism involves the formation of a new reaction intermediate OH_FeCe@CNT due to the combination of one more proton and electron with the O_FeCe@CNT intermediate. Here, the activated oxygen atom reacts with one proton and electron to form a hydroxyl group (OH^-), which remains attached to the surface of the FeCe@CNT material. This reaction step occurred with an energy cost of $\Delta E = -0.98$ eV, as tabulated in Table 2. The equilibrium structure of the OH_FeCe@CNT intermediate is depicted in Fig. 6a. The optimized lattice parameters of the OH_FeCe@CNT material are $a = b = 18.78$ Å, $c = 2.54$ Å and $\alpha = \beta = 90°$, $\gamma = 120°$, respectively. In the OH_FeCe@CNT reaction intermediate, the average values of the C–C and C–O bond distances are 1.79 Å and 1.44 Å, respectively. In contrast, the optimized O–H bond length is 0.96 Å computed by the DFT-D method in the present investigation. The electronic band structure of the OH_FeCe@CNT reaction intermediate was computed using a high symmetric Γ–K–M–L–A–H–L–Γ path, followed by the original k-path of the CNT to compare the results. Both the electronic band structure and TDOS calculations of the OH_FeCe@CNT intermediate are depicted in Fig. 6b.

Table 1 The equilibrium lattice parameter and symmetry of all the reaction intermediates involved in the associative mechanism of ORR

System	Lattice parameters (in Å)	Lattice angles (in degrees)	Space group symmetry	Average bond lengths (in Å)		
				C–C	C–O	O–H
FeCe@CNT	$a = b = 21.65$, $c = 2.49$	$\alpha = \beta = 90$, $\gamma = 120$	$P\bar{6}$	1.43	—	—
O_2_FeCe@CNT	$a = b = 21.59$, $c = 2.51$	$\alpha = \beta = 90$, $\gamma = 120$	$P\bar{6}$	1.44	2.87	—
OOH_FeCe@CNT	$a = b = 21.85$, $c = 2.50$	$\alpha = \beta = 90$, $\gamma = 120$	$P\bar{6}$	1.61	1.46	0.97
O_FeCe@CNT	$a = b = 22.84$, $c = 2.48$	$\alpha = \beta = 90$, $\gamma = 120$	$P\bar{6}$	1.48	1.35	—
OH_FeCe@CNT	$a = b = 18.78$, $c = 2.54$	$\alpha = \beta = 90$, $\gamma = 120$	$P\bar{6}$	1.79	1.44	0.96

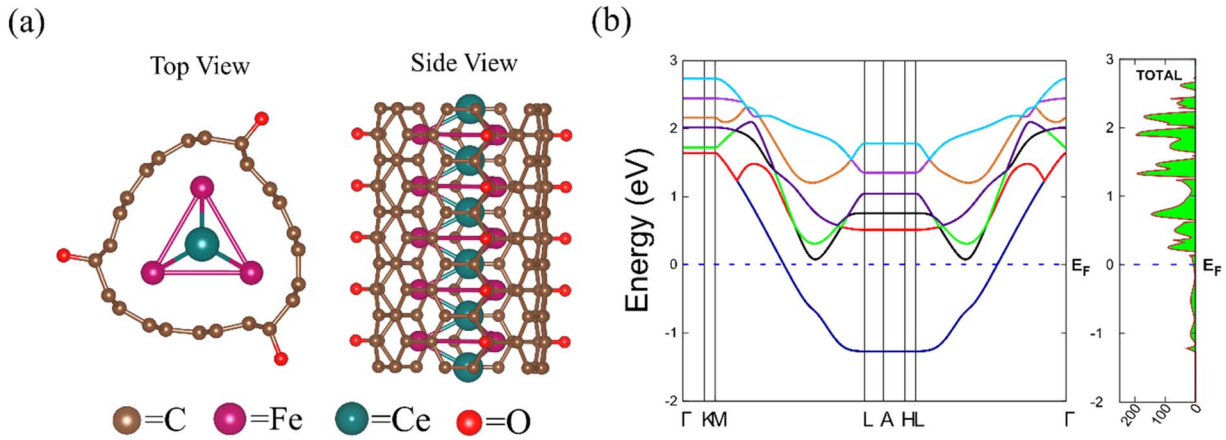

Fig. 5 (a) Top view and side view of the equilibrium structure of O_FeCe@CNT, and (b) the band structure and the total DOS of the O_FeCe@CNT intermediate.

Table 2 Relative adsorption energy of various intermediates during the associative pathway of ORR on the surface of the FeCe@CNT material

ORR steps	Adsorption energy ΔE (in eV)	Relative adsorption energy (in eV)
[FeCe@CNT] → [O_2_FeCe@CNT]	−1.67	−1.67
[O_2_FeCe@CNT] → [OOH_FeCe@CNT]	−0.10	−1.78
[OOH_FeCe@CNT] → [O_FeCe@CNT]	−2.59	−4.37
[O_FeCe@CNT] → [OH_FeCe@CNT]	−0.98	−5.35
[OH_FeCe@CNT] → [FeCe@CNT]	−0.46	−5.81

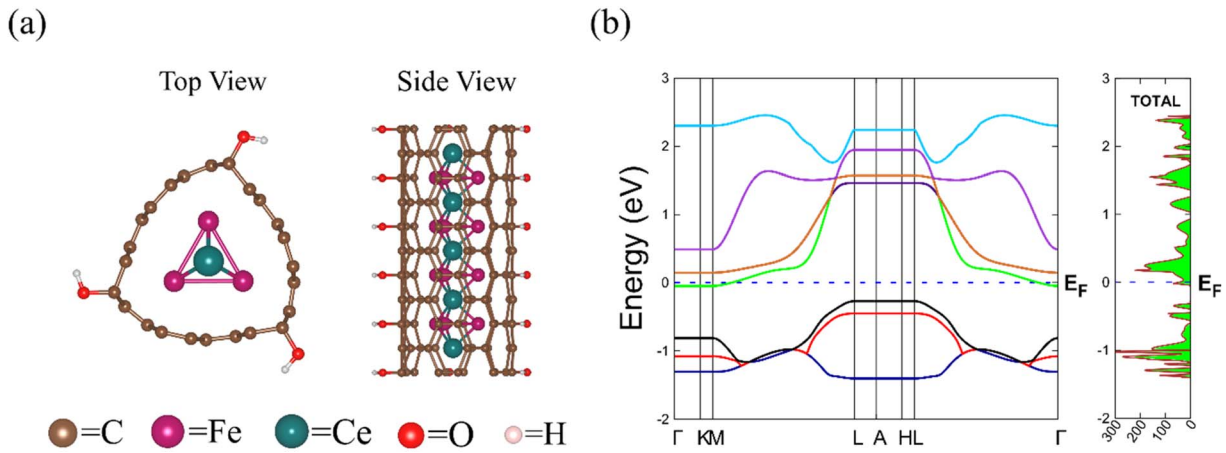

Fig. 6 (a) Equilibrium structure depicting the top and side views of OH_FeCe@CNT, and (b) the electronic band structure and total DOS of the OH_FeCe@CNT intermediate.

Step 5. second H_2O molecule formation. In the last step of the ORR mechanism, one more electron and proton react simultaneously with the OH_FeCe@CNT intermediate to produce a second water (H_2O) molecule with an energy cost of $\Delta E = -0.46$ eV. Hence, in the associative mechanism of ORR, a total number of four protons (H^+) and four electrons (e^-) are used for the reduction of the O_2 molecule to form two H_2O molecules. The adsorption energy profile for all the reaction intermediates of the associative pathway occurring on the surface of the FeCe@CNT material is represented in Fig. 7. The adsorption energy (ΔE) and relative adsorption energy of all the reaction intermediates of ORR are listed in Table 2. In the adsorption energy profile, all the reaction intermediates steps are negative and downhill, which proves the excellent energetics and thermodynamic favorability of the FeCe@CNT material for the O_2 reduction reaction. The ORR mechanism will follow a $4e^-$ path selectivity *via* associative pathway on the surface of the FeCe@CNT material. The ORR overpotential ($\eta = \Delta G_{max}/e^- + 1.23$ V) was found to be 1.13 eV; as the value of $\Delta E \sim \Delta G = -0.46$ eV in the last step to form the H_2O.

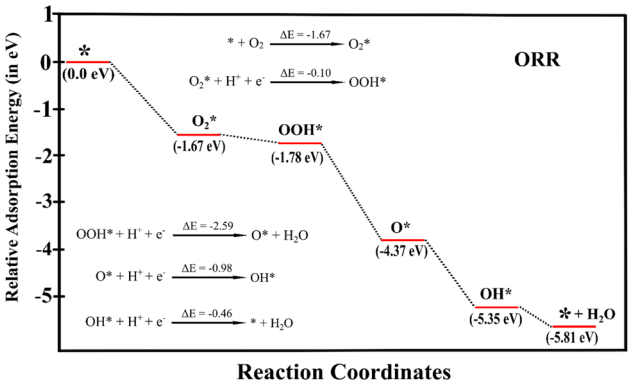

Fig. 7 Adsorption energy profile of various reaction intermediates of the associative mechanism of ORR on the surface of the FeCe@CNT material.

Liu *et al.* proposed that the Pt (111) surface exhibited ORR activity with an overpotential of about 1.04 V.[72] In our recent study, we found that the cobalt-platinum encapsulated carbon nanotube (CoPt@CNT) exhibited an ORR overpotential of about 1.07 V.[31] It was found that the ORR overpotential on real conventional Pt/C could be 0.69–1.68 V.[73] Nitrogen-doped graphene/multi-walled CNT composite as a cathode catalyst has shown an ORR overpotential of 0.43 V.[74] FeCe@CNT exhibits a slightly higher overpotential (1.13 eV) compared to the pristine Pt and Pt-based electrocatalysts. However, the ORR activity is comparable to the other reported electrocatalysts, which have relatively moderate overpotentials. FeCe@CNT could not perform better than the pure Pt catalyst with low overpotential. However, it can be used as an alternative cathodic material in the fuel cells for efficiently catalyzing the ORR with the reduced cost. Niu *et al.* experimentally showed that the CoNi@NCNT material exhibited excellent electrocatalytic activity for ORR and OER. The high catalytic performance of CoNi@NCNT is due to the synergistic effects between the NCNT and the encapsulated CoNi nanoparticles.[24] Singh and Pakhira found that the stability and electrocatalytic activity of the CNT surface were enhanced by encapsulating the Co nanocluster inside the SWCNT.[30] Similarly, the FeCe@CNT material has shown enhanced stability and ORR activity achieved due to nanocluster encapsulation by the CNT wall, which agrees with other reported studies.

The novelty of the present work lies in the first principles-based quantum mechanical study of the FeCe@CNT material towards the ORR, which can be useful for fuel cells application in the near future. The present work involves the study of the structural and electronic properties of the FeCe@CNT with their ORR intermediates, and the present study reveals the ORR pathways and suitability towards the electrode material. Here, the DFT-D method was employed to investigate the equilibrium structure, electronic band structure, TDOS, and band gap of the

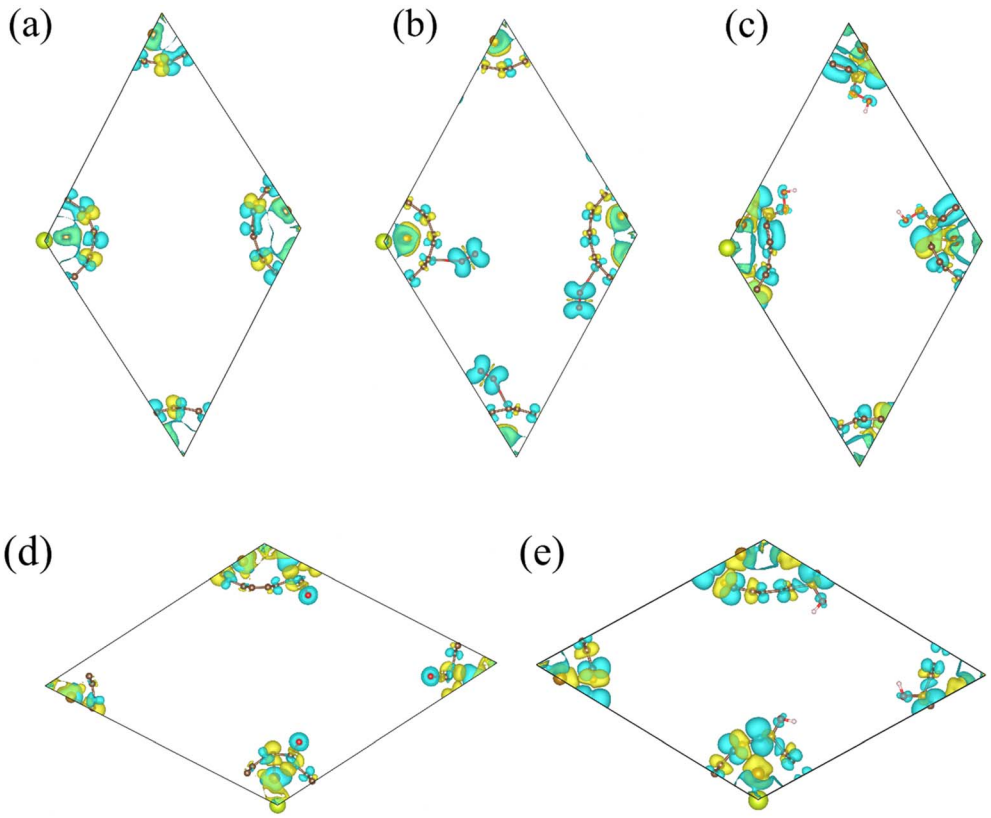

Fig. 8 Spin density plot of all the reaction intermediates of the ORR mechanism: (a) pure FeCe@CNT, (b) O_2_FeCe@CNT, (c) OOH_FeCe@CNT, (d) O_FeCe@CNT and (e) OH_FeCe@CNT. The sky-blue color represents positive α spin-up electron density, and the yellow color represents negative β spin-down electron density.

subject material. This setup gives reliable and precise details on the electronic structure and catalytic activity of the FeCe@CNT material. It improves accuracy for weak interactions that are key to ORR catalysts. In the present study, we have explored the electronic properties of each ORR intermediate while computing their adsorption energy (ΔE), which is very crucial for understanding the catalytic performance of the subject material. Our results show strong potential for improving renewable energy technologies like fuel cells. We hope that our findings provide a simple and new way to explore new catalysts for practical use in fuel cells and renewable energy. This advances ORR catalyst development for practical applications in fuel cells.

Spin density calculation

In this work, electron spin density calculations were performed for all the reaction intermediates of the ORR involved in the associative mechanism. Spin density is the difference in the distribution of spin-up (α) and spin-down (β) electrons in a material. The location of unpaired electrons can be found through spin density calculation and their contribution to the overall magnetic behavior can be estimated. The transfer of electrons and charge can be better understood by learning the electron spin density calculations with analysis.[54,75–78] The DFT-D3 method was used to compute the electron spin density computations of the ORR intermediates with the pristine FeCe@CNT material in the present study. The Fe atom encapsulated at the center of the CNT is the primary source of spin density due to its unpaired 3d electrons, which strongly interact with the surrounding Ce atoms and the π-system of CNT. The Ce atoms with their partially filled 4f and 5d orbitals hybridize with the Fe 3d orbital and help to spread the spin density more effectively across the surface of the subject material. When an O_2 molecule get adsorbed on the outer surface of the CNT, it is not directly bonded to the encapsulated Fe atom. Still, the spin density plots in Fig. 8 clearly show that the electron density from Fe through Ce and the CNT spreads toward O_2, which weakens its O–O bond and activates it for the subsequent proton-electron transfer steps of the ORR. The contribution of Fe and Ce underscores their cooperative role in enhancing the catalytic efficiency of the FeCe@CNT material. Fig. 8a–e depicts the spin density plots of each reaction intermediates involved in the ORR mechanism. In the spin density plots, the sky-blue region represents spin-up (α) density, whereas the spin-down (β) density is represented by yellow color. The spin density plots in Fig. 8 signify that there is a transfer of unpaired electrons during the ORR.

Conclusions

In the present study, the structural and electronic properties of the pristine FeCe@CNT material have been studied by employing the periodic hybrid DFT-D3 method, considering a vdW crystal model system. Our results reveal that the equilibrium structure of the FeCe@CNT material acquires a stable hexagonal $P\bar{6}$ space group symmetry, and its TDOS confirms a metallic nature, arising primarily from the strong contribution of Fe and Ce d-orbitals near the Fermi level (E_F). This metallic character is crucial for efficient electron transfer, making FeCe@CNT an attractive material for electrocatalytic applications. We have further explored the ORR pathway on the surface of the FeCe@CNT material by evaluating the adsorption energies (ΔE) of key intermediates. The present investigation has found that the adsorption of an O_2 molecule on the surface of FeCe@CNT occurs with an energy cost of -1.67 eV, signifying a spontaneous and energetically favorable activation of O_2 molecules. In this study, we have explored both the associative and dissociative pathways. We found that the dissociative pathway is thermodynamically unfavorable due to its highly positive adsorption energy, indicating that the reaction predominantly proceeds through the associative mechanism. The formation of the OOH intermediate in the associative mechanism is energetically favorable and spontaneous because the energy cost for this step to occur is -0.10 eV. We have explored all the reaction steps of the associative pathway on the FeCe@CNT surface. Our energy calculation, including the adsorption energy and the relative adsorption energy of different reaction intermediates, proves that the active sites on the surface of the FeCe@CNT material are energetically and thermodynamically favorable for ORR. Overall, our findings establish the FeCe@CNT material as a highly promising non-noble-metal catalyst with excellent activity toward the ORR. The cooperative interaction between the Fe and Ce atoms with the CNT enables efficient O_2 activation and ensures favorable stabilization of all the reaction intermediates. This interaction enhances the catalytic performance, while reducing reliance on expensive noble metals such as Pt. Notably, the present study provides fundamental insights into the structural and electronic properties of FeCe@CNT, and underscores its potential as a cost-effective, stable, and sustainable electrocatalyst. The insights gained from this work can guide the rational design of next-generation carbon-supported transition-metal catalysts for clean and green energy conversion technologies, particularly in fuel cells and metal-air batteries. We hope that our current study can be useful in finding more stable, low-cost and efficient electrocatalysts for ORR, which can drive the research towards finding clean and green energy-converting devices.

Author contributions

The manuscript was written through the contributions of all authors. Dr. Srimanta Pakhira (S. P.) developed the research concept with ideas and directed the theoretical calculations. S. P. designed and directed the theoretical calculations. Mr. Dikeshwar Halba (D. H.) carried out most of the DFT calculations, D. H. wrote the manuscript and Mr. Lokesh Yadav (L. Y.) helped Mr. Dikeshwar Halba with writing the manuscript with the DFT calculations. Dr. Srimanta Pakhira supervised the project and edited the manuscript.

Conflicts of interest

The authors have no conflicts of interest.

Data availability

The data supporting this article have been included as part of the supplementary information (SI). Equilibrium geometries with all the data that support the findings of this study are available in the main paper and the SI. The atomic coordinates of the optimized computational models are available in the SI. Supplementary information is available. See DOI: https://doi.org/10.1039/d6ra00601a.

Acknowledgements

We thank the CSIR, Government of India, for providing the research funds under scheme no. 22/0883/23/EMR-II. This work was financially supported by the Science and Engineering Research Board-Department of Science and Technology (SERB-DST), Government of India, under Grant No. CRG/2021/000572. Dr. Srimanta Pakhira acknowledges SERB-DST, Government of India, for providing his Early Career Research Award (ECRA) under project number ECR/2018/000255. Dr. Pakhira also thanks SERB-DST for providing the highly prestigious Ramanujan Faculty Fellowship under scheme number SB/S2/RJN-067/2017 and providing the highly prestigious Core Research Grant (CRG), SERB-DST, Government of India, under the scheme number CRG/2021/000572. Mr. Dikeshwar thanks the CSIR, Government of India, for providing his doctoral fellowship under scheme no. CSIRAWARD/JRF-NET2022/12028. Mr. Lokesh Yadav thanks the CSIR, Government of India, for providing his doctoral fellowship under scheme no. CSIRAWARD/JRF-NET2022/11898. The authors acknowledge SERB-DST (at present Anusandhan National Research Foundation (ANRF)) for providing computing clusters and programs. We extend our thanks to ANRF for providing the funds under the scheme no. ANRF/PAIR/2025/000018/PAIR. We thank Professor Shailesh I. Kundalwal, Department of Mechanical Engineering, Indian Institute of Technology Indore, Simrol, Khandwa Road, Indore, Madhya Pradesh, 453552, India, and Professor Apurba Kumar Das, Department of Chemistry, Indian Institute of Technology Indore, Simrol, Khandwa Road, Indore, Madhya Pradesh, 453552, India, for providing their valuable suggestions to improve the quality of the manuscript.

References

1 S. K. Ghosh and B. K. Ghosh, *Glob. J. Eng. Sci.*, 2020, **5**, 2039–2641.
2 N. Abas, A. Kalair and N. Khan, *Futures*, 2015, **69**, 31–49.
3 Y. Huang, Z. Kuldasheva, S. Bobojanov, B. Djalilov, R. Salahodjaev and S. Abbas, *Environ. Sci. Pollut. Res.*, 2023, **30**, 10854–10866.
4 S. Chu, Y. Cui and N. Liu, *Nat. Mater.*, 2017, **16**, 16–22.
5 X. X. Wang, M. T. Swihart and G. Wu, *Nat. Catal.*, 2019, **2**, 578–589.
6 S. Zhang, M. Chen, X. Zhao, J. Cai, W. Yan, J. C. Yen, S. Chen, Y. Yu and J. Zhang, *Electrochem. Energy Rev.*, 2021, **4**, 336–381.
7 H. A. Gasteiger and N. M. Marković, *Science*, 2009, **324**, 48–49.
8 V. R. Stamenkovic, B. Fowler, B. S. Mun, G. Wang, P. N. Ross, C. A. Lucas and N. M. Markovic, *Science*, 2007, **315**, 493–497.
9 P. Wei, X. Li, Z. He, X. Sun, Q. Liang, Z. Wang, C. Fang, Q. Li, H. Yang, J. Han and Y. Huang, *Chem. Eng. J.*, 2021, **422**, 130134.
10 F. Cheng and J. Chen, *Chem. Soc. Rev.*, 2012, **41**, 2172–2192.
11 D. Halba and S. Pakhira, *ACS Omega*, 2024, **9**, 35614–35626.
12 V. Tripkovic and T. Vegge, *J. Phys. Chem. C*, 2017, **121**, 26785–26793.
13 N. M. Marković and P. N. Ross Jr, *Surf. Sci. Rep.*, 2002, **45**, 117–229.
14 M. K. Debe, *Nature*, 2012, **486**, 43–51.
15 K. Khatri, N. Sharma, H. Joshi and S. Pakhira, *Energy Fuels*, 2025, **39**, 9066–9080.
16 Y. Wang, Y. Li and T. Heine, *J. Am. Chem. Soc.*, 2018, **140**, 12732–12735.
17 Z. Yang, H. Nie, X. Chen, X. Chen and S. Huang, *J. Power Sources*, 2013, **236**, 238–249.
18 J. Wu and H. Yang, *Acc. Chem. Res.*, 2013, **46**, 1848–1857.
19 Z. Chen, D. Higgins, H. Tao, R. S. Hsu and Z. Chen, *J. Phys. Chem. C*, 2009, **113**, 21008–21013.
20 L. M. Ericson, H. Fan, H. Peng, V. A. Davis, W. Zhou, J. Sulpizio, Y. Wang, R. Booker, J. Vavro, C. Guthy, A. N. G. Parra-Vasquez, M. J. Kim, S. Ramesh, R. K. Saini, C. Kittrell, G. Lavin, H. Schmidt, W. W. Adams, W. E. Billups, M. Pasquali, W.-F. Hwang, R. H. Hauge, J. E. Fischer and R. E. Smalley, *Science*, 2004, **305**, 1447–1450.
21 A. B. Dalton, S. Collins, E. Muñoz, J. M. Razal, V. H. Ebron, J. P. Ferraris, J. N. Coleman, B. G. Kim and R. H. Baughman, *Nature*, 2003, **423**, 703.
22 Q. Zhang, J.-Q. Huang, W.-Z. Qian, Y.-Y. Zhang and F. Wei, *Small*, 2013, **9**, 1237–1265.
23 J. Le Xie, C. X. Guo and C. M. Li, *Energy Environ. Sci.*, 2014, **7**, 2559–2579.
24 W. Niu, S. Pakhira, K. Marcus, Z. Li, J. L. Mendoza-Cortes and Y. Yang, *Adv. Energy Mater.*, 2018, **8**, 1800480.
25 T. Li, G. Luo, K. Liu, X. Li, D. Sun, L. Xu, Y. Li and Y. Tang, *Adv. Funct. Mater.*, 2018, **28**, 1805828.
26 H. Tabassum, A. Mahmood, B. Zhu, Z. Liang, R. Zhong, S. Guo and R. Zou, *Energy Environ. Sci.*, 2019, **12**, 2924–2956.
27 Y. Yao, H. Chen, C. Lian, F. Wei, D. Zhang, G. Wu, B. Chen and S. Wang, *J. Hazard. Mater.*, 2016, **314**, 129–139.
28 W. Yang, X. Liu, X. Yue, J. Jia and S. Guo, *J. Am. Chem. Soc.*, 2015, **137**, 1436–1439.
29 Y. Zhao, D. Liu, Y. Tian, Y. Zhai, C. Tian, S. Li, T. Xing, Z. Li and P. Dai, *Nanomaterials*, 2023, **13**, 2439.
30 A. Singh and S. Pakhira, *Energy Fuels*, 2024, **38**, 11837–11851.
31 D. Halba, A. Ojha and S. Pakhira, *ACS Appl. Energy Mater.*, 2025, **8**, 7948–7962.
32 H. Zhang, Y. Wang, D. Song, L. Wang, Y. Zhang and Y. Wang, *Nanomaterials*, 2023, **13**, 1921.
33 T. Masuda, H. Fukumitsu, K. Fugane, H. Togasaki, D. Matsumura, K. Tamura, Y. Nishihata, H. Yoshikawa, K. Kobayashi, T. Mori and K. Uosaki, *J. Phys. Chem. C*, 2012, **116**, 10098–10102.

34 Z. Wang, S. Xiao, Z. Zhu, X. Long, X. Zheng, X. Lu and S. Yang, *ACS Appl. Mater. Interfaces*, 2015, **7**, 4048–4055.
35 L. Kashinath and K. Byrappa, *Front. Chem.*, 2022, **10**, 889579.
36 J. Bi, X. Zhai, J. Chi, X. Wu, S. Chen, X. Wang and L. Wang, *Electrochem. Sci. Adv*, 2022, **2**, e2100082.
37 L. Yadav and S. Pakhira, *J. Mater. Chem. C*, 2023, **11**, 15215–15232.
38 P. A. Christensen, A. Hamnett and D. Linares-Moya, *Phys. Chem. Chem. Phys.*, 2011, **13**, 5206–5214.
39 V. Kumar and S. Pakhira, *Mol. Syst. Des. Eng.*, 2023, **8**, 1060–1074.
40 A. D. Becke, *J. Chem. Phys.*, 1992, **96**, 2155–2160.
41 A. Singh and S. Pakhira, *Energy Fuels*, 2023, **37**, 567–579.
42 R. Dovesi, F. Pascal, B. Civalleri, K. Doll, N. M. Harrison, I. Bush, P. D'Archo, Y. Noel, M. Rerat, P. Carbonniere, M. Causa, S. Salustro, V. Lacivita, B. Kirtman, A. M. Ferrari, F. S. Gentile, J. Baima, M. Ferrero, R. Demichelis and M. D. L. Pierre, *J. Chem. Phys.*, 2020, **152**, 204111.
43 G.-C. Wang, L. Jiang, X.-Y. Pang and J. Nakamura, *J. Phys. Chem. B*, 2005, **109**, 17943–17950.
44 V. Kumar, D. Halba, S. N. Upadhyay and S. Pakhira, *Langmuir*, 2024, **40**, 14872–14887.
45 S. Pakhira and S. N. Upadhyay, *Sustain. Energy Fuels*, 2022, **6**, 1733–1752.
46 S. Pakhira and J. L. Mendoza-Cortes, *J. Phys. Chem. C*, 2020, **124**, 6454–6460.
47 J. Kullgren, C. W. M. Castleton, C. Müller, D. M. Ramo and K. Hermansson, *J. Chem. Phys.*, 2010, **132**, 54110.
48 X. Zhang, L. Zhu, Q. Hou, J. Guan, Y. Lu, T. W. Keal, J. Buckeridge, C. R. A. Catlow and A. A. Sokol, *Chem. Mater.*, 2023, **35**, 207–227.
49 H. J. Monkhorst and J. D. Pack, *Phys. Rev. B*, 1976, **13**, 5188.
50 S. Salustro, A. M. Ferrari, R. Orlando and R. Dovesi, *Theor. Chem. Acc.*, 2017, **136**, 1–13.
51 S. Pakhira, K. P. Lucht and J. L. Mendoza-Cortes, *J. Phys. Chem. C*, 2017, **121**, 21160–21170.
52 K. Momma and F. Izumi, *J. Appl. Crystallogr.*, 2011, **44**, 1272–1276.
53 S. N. Upadhyay and S. Pakhira, *J. Mater. Chem. C*, 2021, **9**, 11331–11342.
54 W. Niu, S. Pakhira, G. Cheng, F. Zhao, N. Yao, J. L. Mendoza-Cortes and B. E. Koel, *Nat. Mater.*, 2024, **23**, 1704–1711.
55 K. Liang, S. Pakhira, Z. Yang, A. Nijamudheen, L. Ju, M. Wang, C. I. Aguirre-Velez, G. E. Sterbinsky, Y. Du, Z. Feng, J. L. Mendoza-Cortes and Y. Yang, *ACS Catal.*, 2019, **9**, 651–659.
56 S. N. Upadhyay, D. Halba, L. Yadav and S. Pakhira, *Langmuir*, 2023, **39**, 17700–17712.
57 Y. Lei, S. Pakhira, K. Fujisawa, X. Wang, O. O. Iyiola, N. Perea López, A. Laura Elías, L. Pulickal Rajukumar, C. Zhou, B. Kabius, N. Alem, M. Endo, R. Lv, J. L. Mendoza-Cortes and M. Terrones, *ACS Nano*, 2017, **11**, 5103–5112.
58 K. A. Samawi, E. A.-A. Salman, H. A. Hasan, H. M. A. Mahmoud, S. M. Mohealdeen, G. Abdulkareem-Alsultan, E. Abdulmalek and M. F. Nassar, *Mol. Syst. Des. Eng.*, 2024, **9**, 464–476.
59 Y. Xiao, W. Wang and Q. Wu, *Int. J. Hydrogen Energy*, 2020, **45**, 3948–3958.
60 Y. Liu, H. Jiang, Y. Zhu, X. Yang and C. Li, *J. Mater. Chem. A*, 2016, **4**, 1694–1701.
61 S. Kumar, R. Kumar, N. Goyal, A. Vazhayil, A. Yadav, N. Thomas and B. Sahoo, *ACS Appl. Nano Mater.*, 2024, **7**, 7865–7882.
62 S. Liang and C. Liang, *Materials*, 2019, **12**, 243.
63 D. Zhang, R. Ding, C. Zhang, Y. Tang, T. Yuan, Q. Dong, L. Bi, S. Shi and Y. He, *Langmuir*, 2022, **38**, 9310–9320.
64 L. Wang, X. Liu, K. Su, W. Liu, F. Niu, X. Li, H. Yue, H. Dong, S. Yang and Y. Yin, *ACS Appl. Nano Mater.*, 2024, **7**, 22855–22864.
65 J. Zhang, J.-O. Müller, W. Zheng, D. Wang, D. Su and R. Schlögl, *Nano Lett.*, 2008, **8**, 2738–2743.
66 Q. Liu, F. Wang, E. Hu, R. Hong, T. Li, X. Yuan, X.-B. Cheng, N. Cai, R. Xiao and H. Zhang, *iScience*, 2022, **25**, 104855.
67 W. Wan, S. Wei, J. Li, C. A. Triana and Y. Zhou, *J. Mater. Chem. A*, 2019, **7**, 15145–15155.
68 D. Deng, L. Yu, X. Chen, G. Wang, L. Jin, X. Pan, J. Deng, G. Sun and X. Bao, *Angew. Chem., Int. Ed.*, 2013, **52**, 371–375.
69 H. Ulbricht, G. Moos and T. Hertel, *Phys. Rev. B*, 2002, **66**, 75404.
70 X. Chen, R. Hu and F. Bai, *Materials*, 2017, **10**, 549.
71 A. V Kuzmin and B. A. Shainyan, *ACS Omega*, 2021, **6**, 374–387.
72 J. Liu, M. Jiao, L. Lu, H. M. Barkholtz, Y. Li, Y. Wang, L. Jiang, Z. Wu, D. Liu, L. Zhuang, C. Ma, J. Zeng, B. Zhang, D. Su, P. Song, W. Xing, W. Xu, Y. Wang, Z. Jiang and G. Sun, *Nat. Commun.*, 2017, **8**, 15938.
73 J. K. Nørskov, J. Rossmeisl, A. Logadottir, L. Lindqvist, J. R. Kitchin, T. Bligaard and H. Jónsson, *J. Phys. Chem. B*, 2004, **108**, 17886–17892.
74 J. Shui, M. Wang, F. Du and L. Dai, *Sci. Adv.*, 2015, **1**, e1400129.
75 G. Bruno, G. Macetti, L. Lo Presti and C. Gatti, *Molecules*, 2020, **25**, 3537.
76 S. N. Upadhyay, V. Kumar, N. Sharma and S. Pakhira, *ACS Appl. Energy Mater.*, 2025, **8**, 8937–8949.
77 A. Singh and S. Pakhira, *ACS Appl. Energy Mater.*, 2025, **8**, 1544–1560.
78 L. Yadav and S. Pakhira, *Energy Fuels*, 2024, **38**, 18800–18813.